**Iraqi Geological Journal**

Journal homepage: https://www.igj-iraq.org

# Petrography and Geochemistry of the Baska Piwaza Ore Mineralization, Halgurd Mountain, Iraqi Kurdistan Region: Insights on the Genesis

**Muhammad A.Ahmed [1,*], Tola A. Mirza [1,*], and Stavros P Kalaitzidis [3]**

1 Department of Geology, College of Science, University of Sulaimani, Sulaimani, Kurdistan Region

2 Department of Geology, University of Patras, GR-26504 Rio Patras, Greece.

* **Correspondence**: tola.merza@univsul.edu.iq , muhammod.ahmed@univsul.edu.iq

Received:
17 February 2023

Accepted:
4 July 2023

Published:
31 August 2023

## Abstract

This paper is the first attempt to study the mineralogical and geochemical features of mineralization hosted within the volcanic rocks of the Baska Piwaza section, at Halgurd Mountain, which is the highest mountain in Kurdistan and the whole of Iraq. The host lithologies in the studied section represent mostly volcanic rocks (basalts to andesites), and secondary sedimentary lithologies, such as radiolarian chert. There are two main stages of oxide and sulfide mineralization that can be recognized under three-time epochs which are early, middle and late stages that caused the formation of oxide and sulfides ore minerals. The most dominant oxide mineral is hematite, with minor contribution of magnetite, goethite, and rutile. In terms of sulfides, pyrite is the predominant mineral phase with secondary contribution of chalcopyrite. The petrographic study and XRD data of the host volcanic rocks reveal that the most abundant minerals are plagioclase, K-feldspar, pyroxene, and amphibole, while the secondary minerals are quartz, calcite, clinochlore, sericite, prehnite, pumpellyite, and muscovite. Additionally, the radiolarian chert is comprised by quartz, hematite, calcite, ankerite, clay minerals, and apatite which is characterized by low silica content and high iron oxide. Low concentration of $TiO_2$ ,and $Fe_2O_3$ are suggesting the quartz vein occurred with the volcanic rocks are formed due to low hydrothermal fluid. Field observation, petrographical and geochemical data indicate that the rocks of the Baska Piwaza section are influenced by hydrothermal alteration, due to the high value of Loss On Ignition (LOI) and the high ratio of alkalis ($Na_2O+K_2O$). Moreover, evidences of chloritization and sericitization of the mafic minerals, and feldspar minerals respectively support the hydrothermal impact.

**Keywords:** Baska Piwaza; Halgurd Mountain; Sulfide and oxide ore minerals; Hydrothermal; Walash volcano-sedimentary rocks

## 1. Introduction

The study area is Baska Piwaza, located in the northeastern region of Halgurd Mountain, which is situated 170 kilometers north of Erbil city with coordinates 36° 44' 8.68" N, 44° 52' 11.94" E to 36° 44' 7.30" N, 44° 51' 46.14" E (Fig. 1). Halgurd Mountain, which has a peak altitude of 3607 meters (as shown in Fig. 1), is the highest mountain in Iraq.

The central part of the Alpine-Himalayan Orogenic-Metallogenic Belt in the Kurdistan Region hosts various metallic mineralization in diverse rock units (Jasim and Goff, 2006). It remains one of the

DOI: 10.46717/igj.56.2B.9ms-2023-8-18

least understood and least explored geological domains of the Kurdistan Region. This study is the first attempt to understand the mineralization of Halgurd Mountain. Halgurd Mountain is composed of rock belonging to the Walash and Naopurdan Group. Bolten (1958) for the first time described the Walash Volcano – Sedimentary Group at Walash village, under the name of Walash Volcanic Series, since it is composed mostly by volcanic rocks.

Al-Bassam (2013) defined three metallogenetic periods; the Triassic-Jurassic, Late Cretaceous, and Paleogene-age. Based on the tectonic structure and metallogenic characteristics, Kurdistan is divided to two metallogenic regions, these of Imbricate Zone (IZ) and Zagros Suture Zone (ZSZ), the ZSZ is characterized by magmatic, volcanic, metamorphic, and hydrothermal types of ore minerals. The major mineralization in ZSZ were formed during Cretaceous and Paleogene being related to the tectonic activities at the edges of the Arabian Plate and the final phase of the Neo-Tethys closure and the related igneous emplacements. ZSZ involves three metallogenic districts: the Qulqula – Khwakurk Mn-Fe District, the Shalair Zn-Pb-Fe District, and the Penjween – Walash Cr-Ni-Cu-Fe District. According to Al Bassam (2013), the studied area is located in Penjween-Walash District that is structured by the Qandil Series (Early Cretaceous), basic and ultrabasic igneous complexes (Late Cretaceous) and Walash and Naopurdan Groups (Tertiary). It is characterized by magmatic Cr, Ni, Fe, and Cu, hydrothermal Cu and Ni, (associated with magmatism), contact metasomatic Fe, and marble and asbestos deposits (Al Bassam, 2013).

In a report by the Ministry of Natural Resources (2016) Kurdistan region is divided into seven blocks according to the occurrence of metallic deposits in Kurdistan: Blocks 1 and 2 are in Duhok, Blocks 3 and 4 are in Erbil, and Blocks 5,6 and 7 are in Sulaimani. The studied area belongs to Block 4. Several researches have been conducted in the adjacent areas of Halgurd Mt.; Mohammed (2006) studied the sandstone of Walash and Naopurdan Group in the Qalander area reporting a high percentage of opaque minerals. Koyi (2006) proposed that the volcanic rocks of Walash Volcano-Sedimentary Group are island arc tholeiite and calc alkaline basalts formed during Middle Eocene-Upper- Eocene age and were affected by lower amphibolites facies. Al-Banna and Al-Mutwali (2008) based on the foraminiferal species that existed within the carbonate rocks of Walash Group assigned a Lutetian stage (Middle Eocene) with a ranging 42.5-48 Ma. Ismail et al (2009) studied chromite pods associated with peridotite from the Rayat area, proposing an ophiolite connection. Ali et al (2013) based on $^{40}$ Ar– $^{39}$ Ar dates, proposed an Eocene-Oligocene age (43 to 24 Ma) for Walash and Naopurdan volcanic rocks and recognized metamorphic alteration under greenschist facies conditions. Ali and Aswad (2013) used SHRIMP U-Pb zircon ages from trachytic andesite of Walash volcanic rocks in the Galalah area. The isotope dating revealed two stages of Paleoproterozoic inherited zircon growth. First 1953±39 Ma cores and the second is ca. 1777±28 Ma rims. Ismail et al (2014) studied the PGE in chromitites of the Walash and Naopurdan Group in the Qalander area, suggesting two stages of chromitite formation; the first stage represents S-saturated peridotite melt that produced high-Al chromitites of MORB affinity, while the second stage is S-undersaturated boninitic melt that produced high-Cr chromitites of arc affinity. Ahmed et al (2020) studied the podiform chromitites that are hosted by serpentinized harzburgites of the Rayat ophiolite in the northeastern of Iraq, and they concluded that these chromitites have a boninitic magmatic origin, formed within the suprasubdution zone in the fore-arc setting. Pirouei et al (2020a, b) studied the occurrence of listvenite bodies and listvenite-associated fuchsite formed by hydrothermal alteration of the Cr-rich serpentinized peridotite within the Walash Series close to the Rayat area. Finally, Pirouei et al (2021) identified sulfide and gossanite-like mineralization in the Rayat area, proposing that the mineralization was formed due to hydrothermal, microbial, and alteration processes.

The objective of this article is to study the petrographical, mineralogical and geochemical features of the mineralization hosted within the volcanic rocks outcropping at the Baska Piwaza section in

Halgurd Mountain (Fig. 1). The aim of the study is to provide an initial genetical aspect for the mineralization.

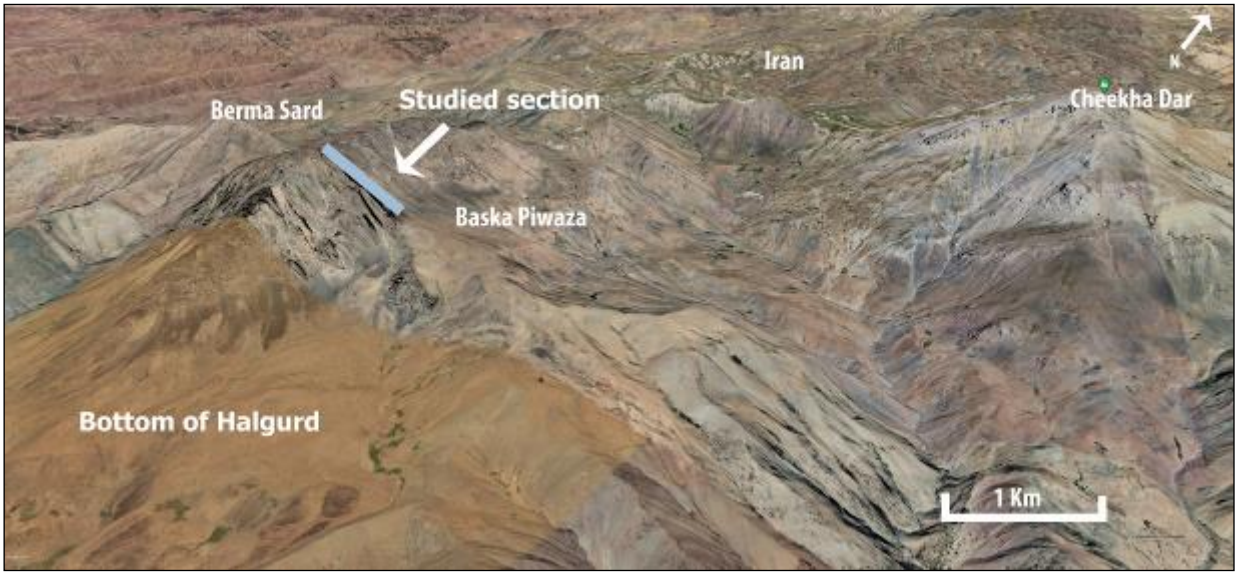


**Fig. 1.** A satellite image (Google Earth) showing the Baska Piwaza study area.

## 2. Geological Setting

Kurdistan Region occupies the north and north-eastern part of Iraqi territory; Iraq itself is located within the northern part of the Arabian Plate, and only a very limited portion not more than five percent extends into the Eurasian (Iranian) Plate (Jassim and Goff, 2006; Fouad, 2015). According to the tectonic division of Iraq by Jassim and Goff (2006), there are four zones in the Kurdistan Region, namely the Foothill, High Folded, Imbricate, and Suture Zones (Fig. 2a). The suture Zone corresponds to locations of the continuous collision between the Iranian and the Arabian, and the Turkish and the Arabian micro-continents, which are located in the northern and northeastern parts of Iraq, respectively (Numan, 1997). The Suture zone is further divided into three tectonic subzones: Qulqula-Khwakurk subzone, Penjween-Walash subzone, and the Shalair subzone (Jassim and Guff, 2006). This classification places the studied area within the Penjween-Walash subzone, which is constructed of two allochthonous thrust sheets, known as the upper and lower allochthonous thrust sheets (Aswad, 1999; Aziz, et al., 2011). The lower allochthonous is composed of Walash-Naopurdan nappe and the upper allochthonous is an ophiolite-bearing terrane (Aswad and Eliase, 1988). The study area in Halgurd Mt, close to Choman town belongs to the lower allochthones of Walash-Naopurdan nappe within the Zagros suture Zone (Fig. 2b). The present study is dealing only with Walash Volcano – Sedimentary Group in Halgurd Mountain. The Walash Volcano – Sedimentary Group is composed of mudstone, siltstone, conglomerate, chert, and the volcanic rocks are basic dykes and volcanic flow to intermediate igneous rocks (Jassim and Goff, 2006). Occasionally intersects of arc-affinity dibasic dykes are also outcropping (Koyi, 2006). Based on stratigraphic relations, an Eocene age was proposed for the Walash Volcano – Sedimentary Group (Bolton 1958, Al-Mehaidi, 1974), however, recent $^{40}Ar$ –$^{39}Ar$ radiometric dating of basaltic rocks revealed an age range of 24 – 43 Ma (Eocene – Oligocene) by Ali et al. (2013).

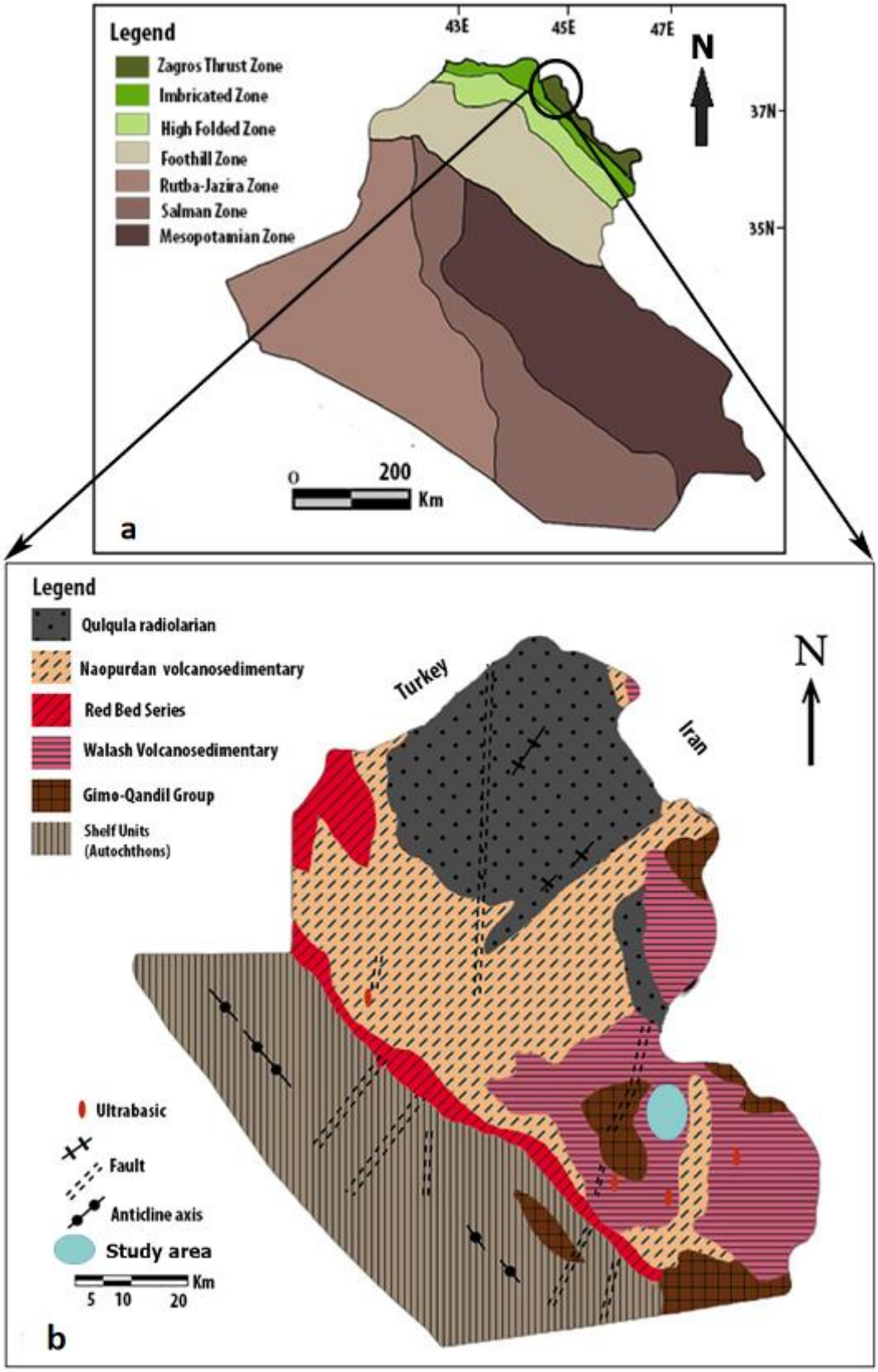


**Fig. 2.** (a) Iraq's Zagros Suture Zone near the Iran-Iraq border is depicted on a simplified geological map (after Moores et al., 2000 and modified by Sissakian, 2000). (b) Detailed geological map of the Rayat area NE-Iraq (modified by Ismail et al., 2014).

## 3. Materials and Methods

Nine samples of representative mineralization and host rock lithologies were collected from the area through two field trips. The thickness of the Baska Piwaza section is approximately 500m; nevertheless, sampling in this area was challenging due to the mountain's steep slope. Fresh samples have been collected from two rock types belonging to the Walash Volcano-Sedimentary Group in the Baska Piwaza section of Halgurd Mountain. The first rock type comprises volcanic lithologies, representing vesicular or amygdaloidal basalts, and basaltic andesite. The second rock type consists of sedimentary lithologies, represented by radiolarian chert lying between the basaltic rocks. Additionally, a sample was taken from the quartz veins that crosscut the volcanic rocks. However, most of the samples were taken from the volcanic igneous rocks due to the presence of mineralization of different types of ore minerals, as well as the appearance of leaching and traces of these mineralization on these rocks in the field. Thin sections were prepared and investigated by using transmitted light polarizing microscope (LEICA DM750P model) at College of Petroleum and Mineral Sciences- Zakho, Duhok Polytechnic University for textures and mineral identifications. Eight mount polished sections were prepared for the mineralization, and studied by using Meiji optical transmitted and reflected light microscopy at Geology Department, University of Sulaimani for texture and mineral identifications.

Determination of the mineralogical composition was performed also on representative powders (Ø < 50 μm) using a Seifert MZVI and a Bruker D8 advance diffractometer with Ni-filtered CuKα radiation. The scanning area covered the $2\theta$ interval 2°–70°, with a scanning step of 0.015° and a time step of 0.1 s. The identification of mineral phases was performed using EVA software and quantified using a Rietveld-based quantification routine of topaz software. XRD analysis was conducted at the Section of Earth Materials, Department of Geology,University of Patras, Greece.

The whole rock geochemical analysis for the determination of the major and minor element contents was carried out on powdered samples using a RIGAKU ZSX PRIMUS II spectrometer equipped with a Rh anode. The XRF analysis was performed in the Laboratory of Electron Microscopy and Microanalysis at t University of Patras, Greece. Loss on ignition (LOI) values are calculated by burning 1g of material for 2 hours at 950 ℃ at University of Patra, Greece by using a Selecta ® muffle furnace (Heiri et al., 2001).

## 4. Results

### 4.1. Field and Petrographical Features of the Host Rock

Two types of rocks are found in the Baska Piwaza section; volcanic lithologies representing vesicular or amygdaloidal basalts, and basaltic andesite (Fig. 3a,b,c, and d), and sedimentary lithologies represented by radiolarian chert lying in between the basaltic rocks (Fig. 3e). Quartz and chlorite veins cross-cut the volcanic rocks (Fig. 3f, g, and h). Both, the volcanic lithologies and the radiolarian chert belong to the Walash Volcano – Sedimentary Group. The mineralization is present either in the form of macroscopically identified ore minerals or appearances of leaching within the volcanic lithologies, which are the main study subject (Fig. 3i).

The microscopic observation revealed that the basalts to andesites of the Baska Piwaza section show a series of textures, including aphanitic (Fig. 4a and b), porphyritic (Fig. 4c), glomeroporphyritic (Fig. 4d), Felty or pilotaxitic (Fig. 4a and b), amygdaloidal textures (Fig. 4e and f). Frequent the amygdales are filled by calcite and iron oxides (Fig. 4g and h), and intergranular textures (Fig. 4i and j). The crystal framework of the studied volcanic rocks represents holo-crystalline to hypo-crystalline grains with cryptocrystalline groundmass. Porphyritic, and intergranular textures are the dominant microstructures of volcanic rocks.

The petrographic study of the volcanic rocks based on the microscopic observation as well as the X-Ray diffraction data reveals that the mineralogical composition and the percentages of the modal mineralogy consists of plagioclase (30-60%), K-feldspar (2-3%), pyroxene (6-20%), amphibole (7-11%), muscovite (0.5-8%), quartz (2-8%), clinochlore (12-41% ), prehnite (1.5-6%), pumpellyite (only found in one sample with 23%), calcite (5-15.5%), ankerite (0.5-1%), clay minerals (0.5%) manifested as a form of a matrix, and opaque minerals (Table 1). The feldspar minerals are altered to sericite (Fig. 4k and l). The opaque minerals of the studied samples appear in the form of phenocrysts, micro phenocrysts, veins, veinlet and a groundmass (Fig. 5 and Table 1). The mineral compositions imply that the studied rocks represent basaltic andesite to andesite rocks, as well as that there is no distinct megascopic discrimination between the two volcanic rocks in the study area.

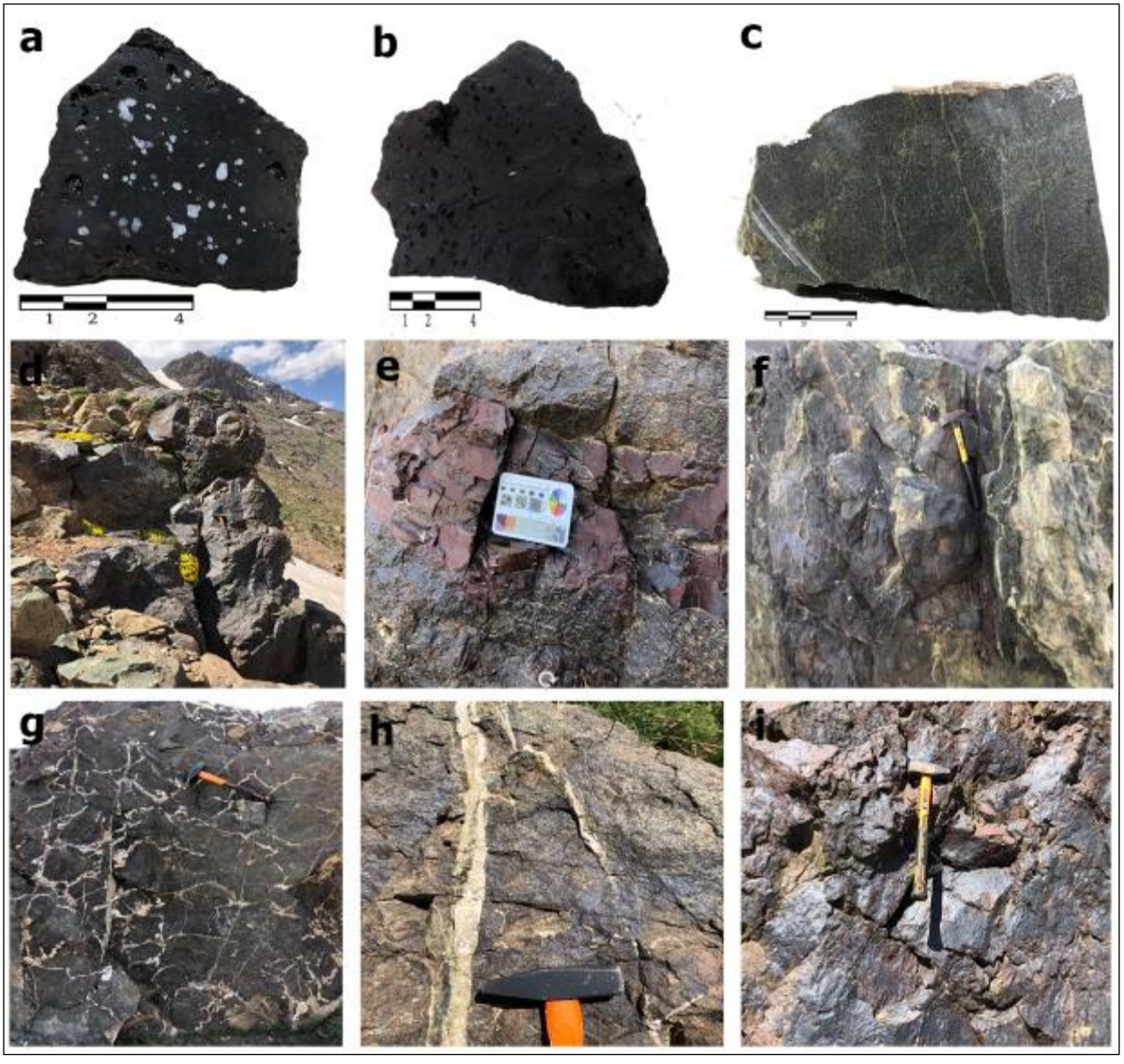


**Fig. 3.** (a) Amygdaloidal basalt. (b) Vesicular basalt. (c) Basaltic andesite. (d) Field photo of outcropping basalt. (e) Radiolarian chert being among basaltic rocks. (f) Veins of chlorite cross cut the rocks. (g and h) Quartz-veins cross cut the rocks. (i) Leaching of oxide and sulfide mineralization.

Clinochlore is present in almost all of the studied samples. It commonly occurs as irregular patches. These patches may be isolated or interconnected (Fig. 4i). Clinochlore also occurs in veins, as cores or

rims in amygdales and as replacement products of pyroxene and igneous amphibole. The color of Clinochlore ranges from colorless to various shades of green or yellow, and the abundance ranges from 12% to nearly 41% in these rocks (Table 1).

The red radiolarian chert occurs with variable thickness, from centimeters to meters and with different mineralogy (Fig. 3e). Amorphous silica is the dominant mineral, with an abundance of about 50% of the total rock volume and hematite percentage is about 23% of the total rock volume (Table 1). Secondary minerals are calcite, ankerite, clay minerals and apatite, (Fig. 5 BP4). Under transmitted microscope they appear red to opaque due to high percentage of iron oxide and clay minerals (Fig. 4m and n).

Quartz veins occurred among the volcanic rocks with different thickness (Fig. 3h). However, there is no any observation for the traces of oxide and sulfide mineralization with the qurtz vein in the studied area. The X-Ray diffraction data reveals that the mineralogical composition of studied quartz vein sample is 100 % quartz mineral (Fig. 5 BP7) and (Table 1 ).

**Table 1.** XRD quantitative data of studied samples.

| **Minerals** | **Volcanic Host Rocks** | | | | | | | **Chert** | **Quartz vein** |
|---|---|---|---|---|---|---|---|---|---|
| | **BP1** | **BP2** | **BP3** | **BP5** | **BP6** | **BP8** | **BP9** | **BP4** | **BP7** |
| Amphibole | 11 | | 10 | 8 | 7 | | | | |
| Clays | | | | 0.5 | | | | 3 | |
| Clinochlore | 41 | 17 | 10 | 27 | 28 | 12 | 20 | | |
| K-feldspar | 3 | | 2 | 2 | | | | | |
| Muscovite | | 3 | 8 | 8 | 0.5 | 1.5 | | | |
| Plagioclase | 35 | 40 | 38 | 30 | 60 | 44 | 60 | | |
| Prehnite | | | | | | 6 | 1.5 | | |
| Pumpellyite | | 23 | | | | | | | |
| Pyroxene | 6 | | 13 | | | 20 | | | |
| Quartz | 3 | 3.5 | 8 | 6 | 2 | 7 | 7 | 50 | 100 |
| Hematite | | 3.5 | 5 | 2 | 0.5 | 4.5 | 6.5 | 23 | |
| Rutile | | | | | | | 1 | | |
| Ankerite | 0.5 | | 1 | 1 | | | | 6 | |
| Calcite | | 10 | 5 | 15.5 | 2 | 5 | 3.5 | 12 | |
| Apatite | | | | | | | | 6 | |
| Pyrite | 0.5 | | | | | | 0.5 | | |

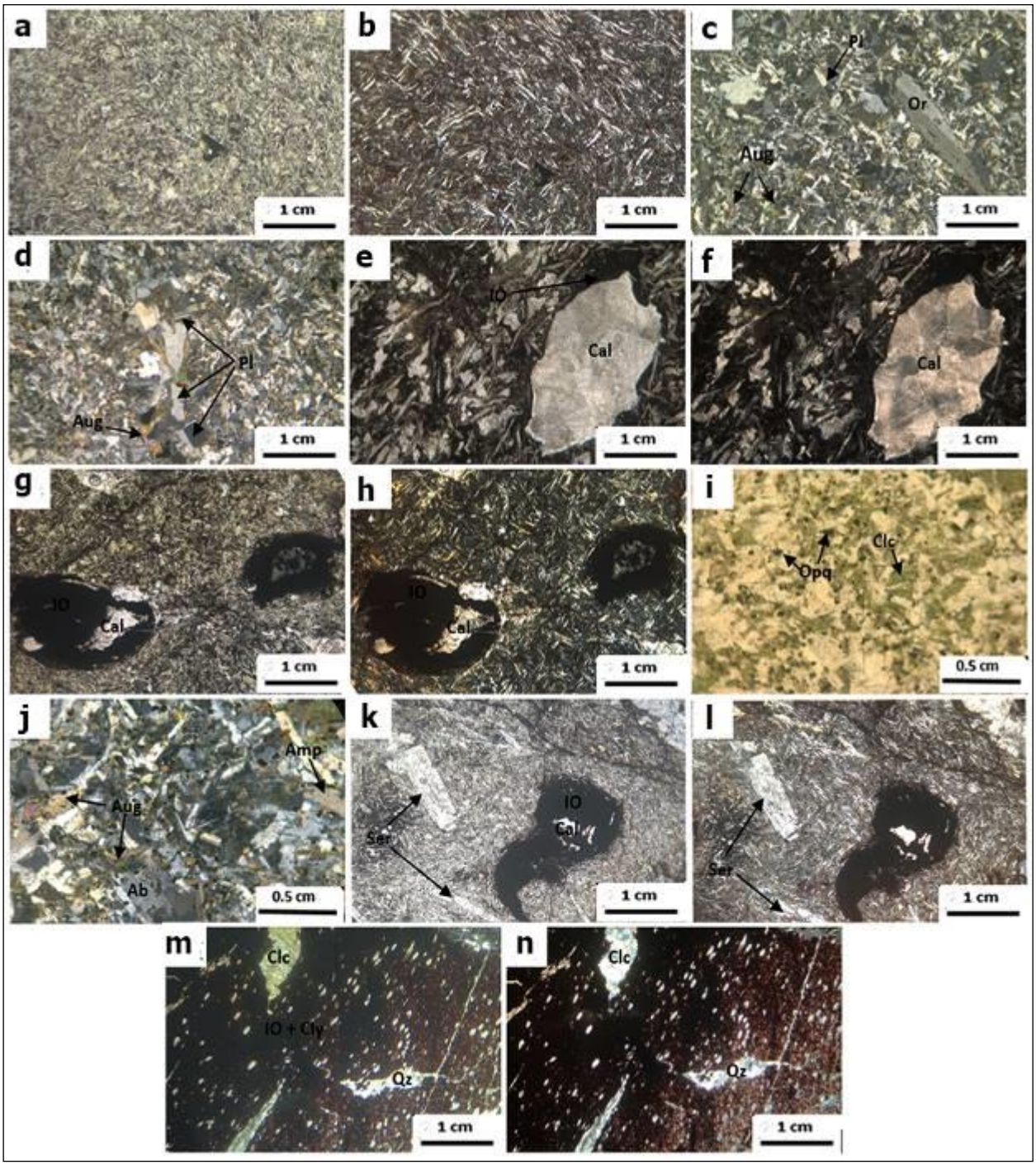


**Fig. 4.** (a) and (b) Aphanitic texture that shows pilotaxitic texture in which the micophenocrysts of the plagioclase are randomly oriented PPL and XPL, respectively. (c) Porphyritic texture the phenocrysts are plagioclase and k-Feldspar, XPL. (d) Glomeroporphyritic texture, XPL. (e ) and (f) Amygdaloidal texture, amygdales are filled by calcite , PPL and XPL, respectively. (g ) and (h) Amygdaloidal texture which are filled by iron oxide, PPL and XPL, respectively. (I) and (j) Intergranular texture the space between plagioclase crystals is occupied by augite, PPL and XPL, respectively. (k) and (l) porphyritic texture that the phenocrysts of plagioclase are altered to sericite, PPL and XPL, respectively. (m) and (n) Radiolarian chert, PPL and XPL, respectively. Clc: Clinochlore, Opq: Opaque minerals, Pl: Plagioclase, Aug: Augite, Cal: Calcite. Ser: Sericite. IO: Iron Oxide, Or: Orthoclase. Qz: Quartz. Mineral abbreviations (from Whitney and Evans, 2010).

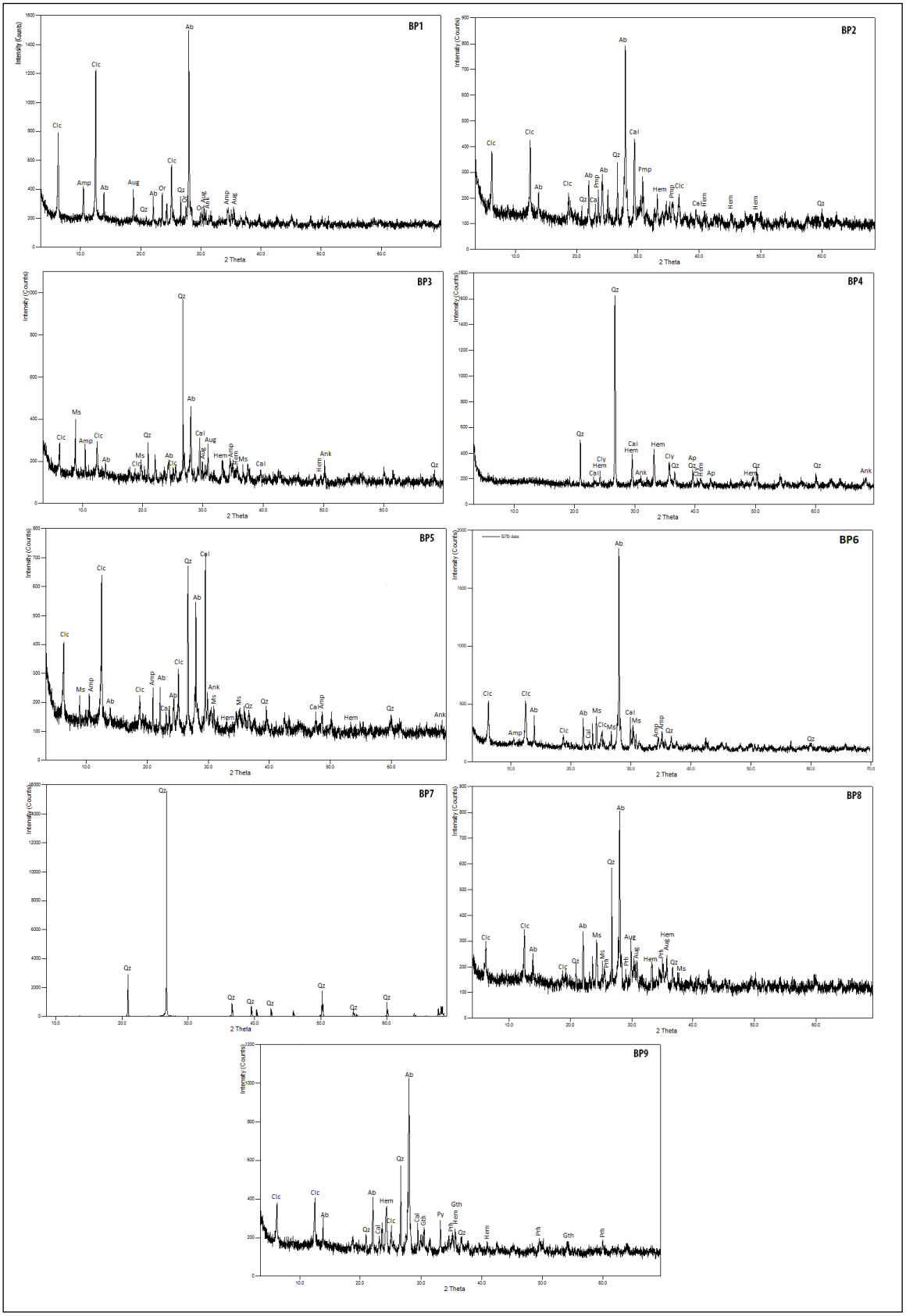


**Fig 5.** Selected X-Ray diffractograms of the studied samples. Ab: Albite, Clc: Clinochlore, Qz: Quartz, Aug: Augite, Hem: Hematite, Cal: Calcite, Ms: Muscovite, Prh: Prehnite, Gth: Goethite, Ank: Ankerite, Amp: Amphibole, Pmp: Pumpellyite, Py: Pyrite, Cly: Clays (mixed layers montmorillonite and illite); mineral abbreviations (from Whitney and Evans, 2010).

### 4.2. Petrographical Features of the Ore Minerals

Two groups of ore minerals were identified in the studied samples under the reflected microscope, representing oxides and sulfide ore minerals. Structurally the sulfide and oxide ore minerals occur as disseminated grains, veins, veinlets and small aggregates. The most abundance oxide ore mineral is hematite, whereas the dominant sulfide minerals are pyrite and chalcopyrite. In terms of gangue minerals, quartz, chlorite, sericite, albite, augite, amphiboles, antigorite, and clay minerals are the most abundant. Conversely, the gangue minerals are distributed as a matrix, representing intergrowth silicate minerals between the sulfide and oxide minerals (Figs. 6, and 7).

Hematite occurs in veins and veinlets as well as in the form of small aggregates, and flow texture in hand specimens (Fig. 6). Microscopically, hematite occurs as small aggregates, filling the amygdales, disseminated, in-filling veins, and lath shape textures in volcanic rocks (Fig. 7a, b, and c). However, hematite in radiolarian chert occurs in veins as well as disseminated within the rock framework (Fig. 7l). The X-Ray diffraction data indicate that hematite in volcanic rocks ranges between 0.5 to 6.5%, whereas in radiolarian chert it reaches up to 23 %. Goethite is less dominant, being characterized by colloform banding with hematite, and is surrounded by a silicate matrix; occasionally goethite seems to have replaced pyrite (Fig. 7d, and e).

Moreover, magnetite occurs as aggregates of euhedral to subhedral grains (Fig. 7j, and k) being disseminated in the host rocks (Fig. 7f, and g). Magnetite is characterized by silicate mineral inclusion and it is frequent cross cut by hematite (Fig.7j, and k).

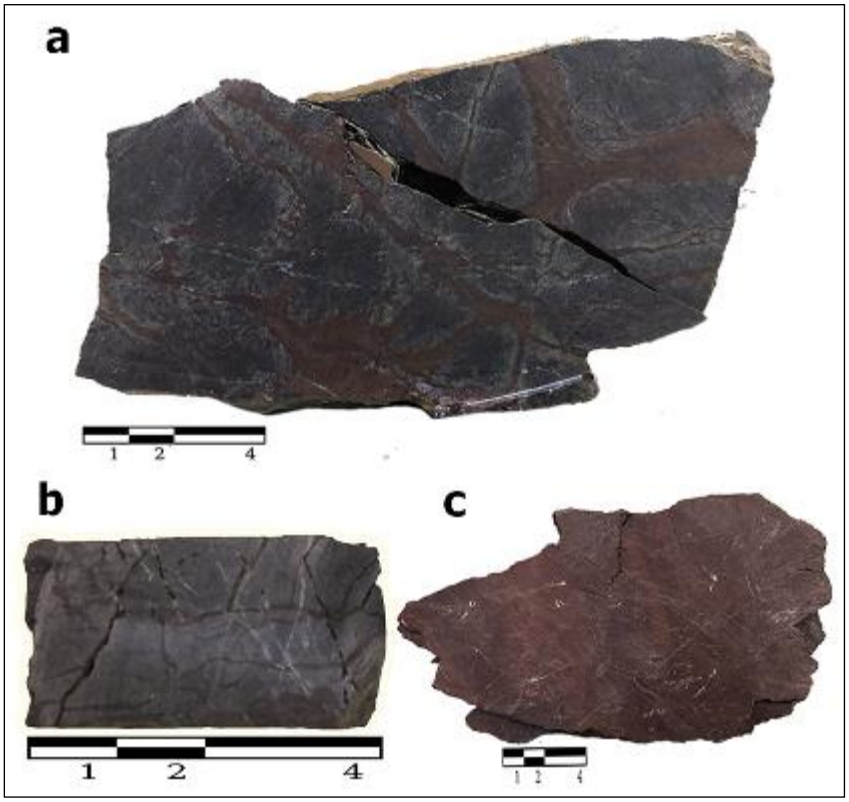


**Fig. 6.** (a) Flow texture of hematite in a basalt sample. (b) veins of hematite in the basaltic rock. (c) Radiolarian chert hosted iron oxide. Hem: Hematite.

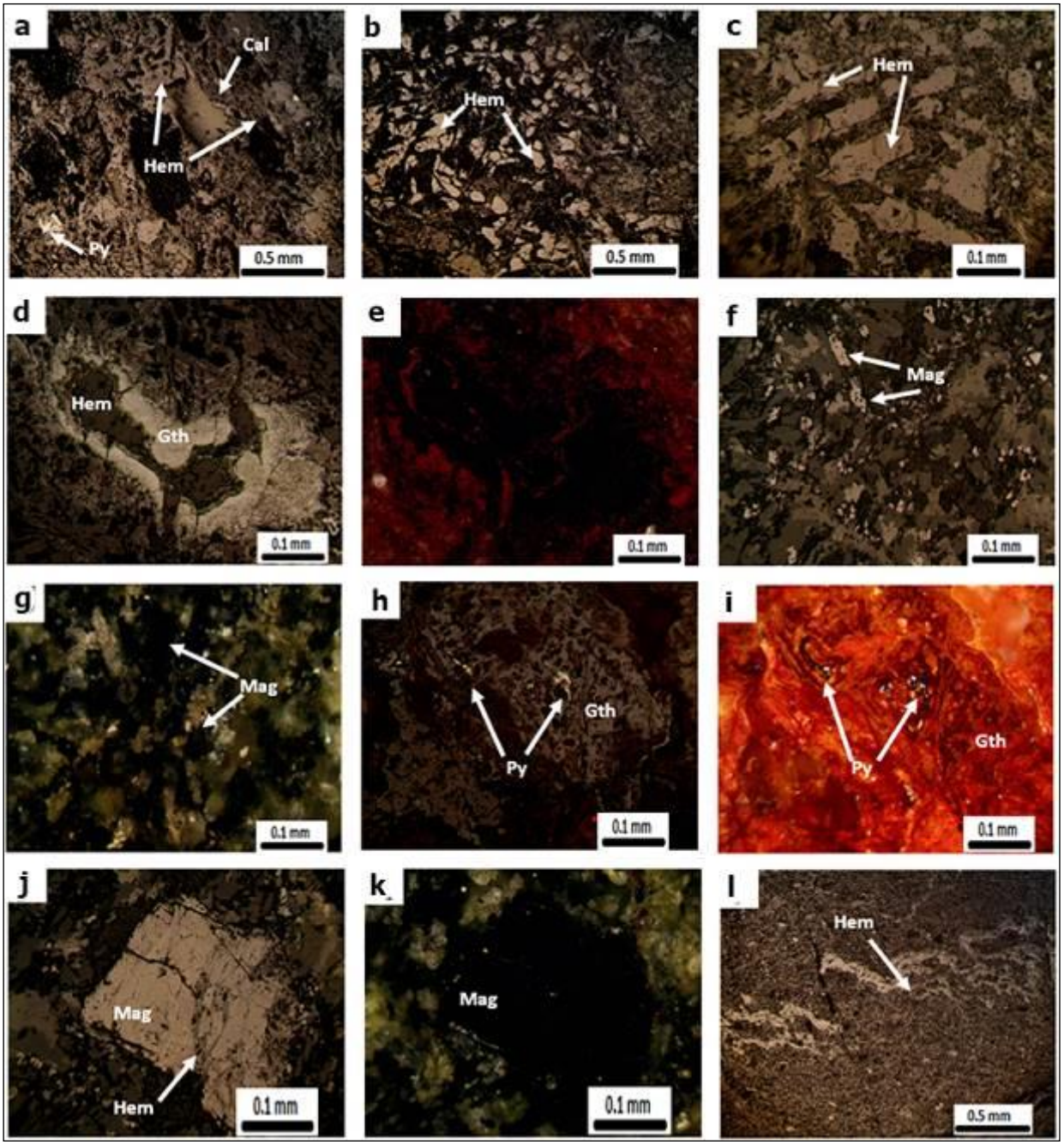


**Fig. 7.** (a) Hematite. (b) disseminated hematite. (c) Lath shaped hematite. (d) colloform goethite under PPl. (e) Colloform goethite under XPL shows red internal reflection. (f) Disseminated magnetite under PPL. (g) Disseminated magnetite under XPL which is isotropic. (h) Goethite replaced pyrite under PPL. (i) Goethite replaced pyrite under XPL. (j) Magnetite grain under PPL. (k) Magnetite grain under XPL which shows isotropy. (l) Hematite in radiolarian chert. Hem: Hematite, Py: Pyrite, Gth: Goethite, Mg: Magnetite.

Sulfide ore minerals are less dominant in the collected studied samples. Generally, they occur as disseminated and small aggregates (Fig. 8). Pyrite is the dominant sulfide minerals, occurring as small grains with white to brass yellow color (Fig. 8a, and b). The grains of pyrite are idiomorphic (Fig. 8c), subhedral, anhedral (Fig. 8d and e), and island replacement textures (Fig. 8f). The coarse grain pyrites are isotropic, characterized by brecciated and cataclastic texture under cross polarized light (Fig. 8c, and e). Pyrite forms replacement texture that are irregularly replaced by hematite and goethite in the rims

(Fig. 7h, and i and Fig. 8d). Chalcopyrite occurs as tiny grains or irregular aggregates and disseminated (Fig. 8g, and h). Chalcopyrite is the only copper bearing mineral were identified in studied samples.

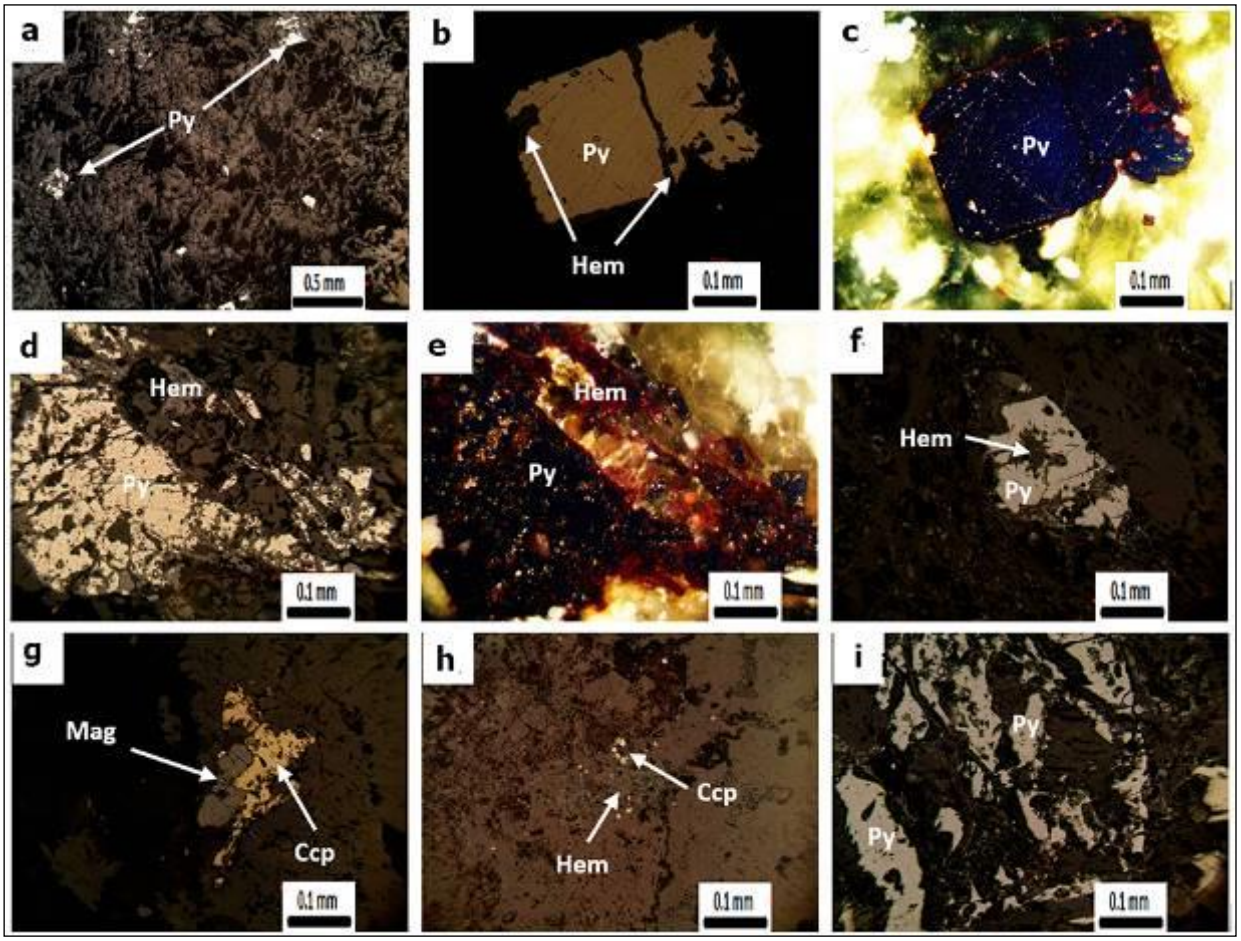


**Fig 8.** (a) Disseminated pyrite. (b) Euhedral pyrite which is cross cut by hematite and also replaced by hematite in the rims PPL. (c) Euhedral pyrite under XPL which is characterized by dark blue anomality of anisotropy. (d) Irregular grain of pyrite that is replaced by hematite Under PPL. (e) Irregular grain of pyrite under XPL. (f) Pyrite altered to hematite forms island texture. (g) Chalcopyrite grain with magnetite. (h) Disseminated chalcopyrite in hematite. (i) White pyrite. Hem: Hematite, Py: Pyrite, Ccp: Chalcopyrite, Mag: Magnetite. Mineral abbreviations (from Whitney and Evans, 2010).

### 4.3. Geochemistry

The results of the whole-rock XRF analyses are presented in Table 2. The range of the major oxides are following: $SiO_2$ 41.9– 52.3 wt.%, CaO 4– 11.4wt.%, $Al_2O_3$ 9.8– 15.8 wt.%, MgO 4.5– 13.5 wt.%, and $Fe_2O_3$ 9.4 - 16.1 wt.%, whereas $K_2O$ varies in the range of 0.03-3.7 wt.%, $Na_2O$ 1.4- 4.7 wt.%, $P_2O_5$ 0.1 - 0.3 wt.%, $TiO_2$ 0.8-2.1 wt.%, and MnO 0.3- 4.7 wt.%. In terms of trace elements, Cr concentration values range between 78 and 371 ppm, Ni 36 – 243 ppm, V 143– 403 ppm, Sr 37 – 217 ppm, Ce <1- 40 ppm, Cu 10 – 758 ppm, Zn 55-511 ppm, Zr <1-177 ppm, Co 22-66 ppm, and Pb 1-231 ppm.The rest elements (Sc, Rb, Y, Nb, Hf, W, La, Ce, and Th) display values mostly below 40 ppm (Table 2).

The concentration of major oxides in radiolarian chert are as follow: $SiO_2$ (45.8 wt.%), CaO (11.3 wt.%), $Al_2O_3$ (6.3 wt.%), MgO (2.3 wt.%), and $Fe_2O_3$(18.4 wt.%), $P_2O_5$ (4.9 wt.%), $TiO_2$ (0.2 wt.%), MnO (2.8 wt.%) and the value of $Na_2O$ and $K_2O$ is (0.3, and 0.2 wt.%) respectively (Table 2, sample BP4). The concentrations of trace elements V, Cr, Ni in radiolarian chert are 148, 115, and 154 ppm, respectively and the other elements (Sc, Co, Cu, Zn, Rb, Sr, Y, Zr, Nb, Ba, Hf, W, Pb, La and Ce) display values mostly below 56 ppm. Moreover, $SiO_2$ in the quartz-vein sample is 98.2 wt.%. The

concentration of other major oxides in quartz-vein sample as follow : MgO and CaO is 0.1 wt.% , $Al_2O_3$ (0.001 wt.%), $Fe_2O_3$(0.04 wt.%), $P_2O_5$ (0.001 wt.%), $TiO_2$ (0.01 wt.%), MnO (0.02 wt.%) and the value of $Na_2O$ and $K_2O$ is (0.06, and 0.004 wt.%) respectively (Table 2 sample BP7). The concentrations of trace elements in quartz-vein sample V, Cr, ,Ni, Cu, Zn, Hf, and Pb are (21, 83, 87, 69, 38, 51, and 34 ppm) respectively, and the other elements Co, Rb, Sr, Y, Zr, Nb, Ba, W, La, Ce, and Th display values mostly below 8 ppm (Table 2 sample BP7). Loss-on-ignition (LOI) values of the volcanic rocks are ranging from 3.7 to 11.1 wt.%, whereas for the radiolarian chert 7.6 wt.% and for the quartz-vein 0.8 wt.% (Table 2).

**Table 2.** Major and trace element contents of the studied samples.

| **Oxide wt. %** | **Volcanic Host Rocks** | | | | | | | **Chert** | **Quartz Vein** |
|---|---|---|---|---|---|---|---|---|---|
| | **BP1** | **BP2** | **BP3** | **BP5** | **BP6** | **BP8** | **BP9** | **BP4** | **BP7** |
| **$SiO_2$** | 50.5 | 44.5 | 52.3 | 41.9 | 50.4 | 45.2 | 50.9 | 45.8 | 98.2 |
| **$TiO_2$** | 2.1 | 1.3 | 1.2 | 0.8 | 1.2 | 1.6 | 2.1 | 0.2 | 0.01 |
| **$Al_2O_3$** | 10.7 | 15 | 13.3 | 9.8 | 12.9 | 15.8 | 12.8 | 6.3 | 0.001 |
| **$Fe_2O_3$** | 16.1 | 10.04 | 9.9 | 9.6 | 9.4 | 12.7 | 12.6 | 18.4 | 0.04 |
| **MnO** | 0.9 | 0.5 | 0.3 | 4.7 | 0.9 | 0.9 | 0.6 | 2.8 | 0.02 |
| **MgO** | 7.4 | 7.5 | 4.5 | 7.9 | 13.5 | 5.7 | 7.5 | 2.3 | 0.1 |
| **CaO** | 4.9 | 10.1 | 7.05 | 11.4 | 4.04 | 9.4 | 4 | 11.3 | 0.1 |
| **$Na_2O$** | 2.8 | 2.9 | 1.4 | 1.8 | 3.5 | 3.4 | 4.7 | 0.3 | 0.06 |
| **$K_2O$** | 0.03 | 0.7 | 3.7 | 0.8 | 0.04 | 0.6 | 0.5 | 0.2 | 0.004 |
| **$P_2O_5$** | 0.3 | 0.2 | 0.2 | 0.1 | 0.1 | 0.3 | 0.2 | 4.9 | 0.001 |
| **LOI-Flux** | 3.7 | 7.8 | 6 | 11.1 | 3.8 | 4.2 | 4.7 | 7.6 | 0.8 |
| **Total** | 99.43 | 100.54 | 99.85 | 99.9 | 99.78 | 99.8 | 100.6 | 100.1 | 99.34 |
| **Trace (ppm)** | | | | | | | | | |
| **Sc** | 19 | 28 | 18 | 24 | 23 | 26 | 22 | 16 | <1 |
| **V** | 403 | 181 | 212 | 143 | 231 | 261 | 344 | 148 | 21 |
| **Cr** | 101 | 316 | 225 | 371 | 353 | 179 | 78 | 115 | 83 |
| **Co** | 66 | 44 | 33 | 40 | 46 | 31 | 22 | 22 | 3 |
| **Ni** | 36 | 181 | 117 | 243 | 213 | 125 | 55 | 154 | 87 |
| **Cu** | 138 | 38 | 86 | 758 | 208 | 74 | 10 | 27 | 69 |
| **Zn** | 124 | 111 | 55 | 511 | 178 | 72 | 77 | 44 | 38 |
| **Rb** | <1 | 24 | 55 | 17 | 13 | 10 | 15 | 0 | 8 |
| **Sr** | 217 | 154 | 173 | 37 | 47 | 79 | 68 | 16 | 7 |
| **Y** | 1.05 | 1.02 | 1.03 | 1.04 | 1.05 | 1.03 | 1.02 | <1 | <1 |
| **Zr** | 177 | 29 | 65 | <1 | 16 | 46 | 58 | 0 | <1 |
| **Nb** | 1.06 | 1.03 | 1.01 | 1.02 | 1.04 | 1.05 | 1.01 | <1 | <1 |
| **Ba** | 133 | 67 | 125 | 101 | 100 | 87 | 93 | 2 | <1 |
| **Hf** | 12 | 35 | 28 | <1 | 16 | 27 | 38 | 28 | 51 |
| **W** | <1 | <1 | <1 | <1 | <1 | <1 | <1 | <1 | 6 |
| **Pb** | 231 | 3 | 1 | 3 | 3 | 2 | 1 | 28 | 34 |
| **La** | 9 | 14 | 12 | <1 | 1 | 9 | <1 | 56 | 2 |
| **Ce** | 40 | 28 | 33 | <1 | 22 | 35 | 38 | 20 | <1 |
| **Th** | 5 | <1 | <1 | <1 | <1 | <1 | <1 | <1 | <1 |
| **Ba/Nb** | 125.47 | 65.05 | 123.76 | 99.02 | 96.15 | 82.86 | 92.08 | | |

## 5. Discussion

### 5.1. Lithological Classification – Petrogenetical Features

By plotting the modal % of the mineral constituents based on XRD data and petrography on the Modal QAPF classification scheme of volcanic rocks by Streckeisen (1978) it is indicated that the studied samples fall in the basalt – andesite field (Fig. 9). The main minerals present are plagioclase, K-feldspar, pyroxene, and amphibole, while additional minerals found are quartz, calcite, clinochlore, sericite, prehnite, pumpellyite, and muscovite. The most abundant mineral is plagioclase, which has tabular shape; however, in several parts plagioclases are altered to sericite (Fig. 4k, and l). Clinochlore (Fig. 4i) is present in almost all of the studied samples. In several occasions pyroxene has been partially or completely replaced by chlorite.

The observed optical features, and more precisely the sericitization of plagioclase, and the chloritization of mafic minerals like pyroxene indicate that the volcanic rocks in the Baska Piwaza section were affected by hydrothermal metamorphism that resulted to the alteration and resorption; The presence of chlorite suggests that these rocks were affected by low-temperature metamorphism at 150°–250°C (Alt et al., 1996).

The only sedimentary rock sample is a radiolarian chert, which is composed mainly by quartz and hematite. According to Montgomery and Kerr (2009) the red coloration of the chert is related to two different origin (1) hydrothermal sediment, reddened by heating and oxidation, was buried by new lava flows and squirted up into the flow, (2) fluids present during the accumulation of the basaltic layer locally oxidized the lava along fractures and produce brick-red in color. As noted, the chert on Baska Piwaza is enriched in $Fe_2O_3$ (Table 2), an indication that the parent was ferruginous hydrothermal sediment (Richards and Boyle, 1986).

Ore microscopy shows that the samples contain sulfides and oxides. The predominant metallic mineral is hematite, which often appears brecciated; this brecciation can be the result of either structural deformation influenced by faults controlling the mineralization activity, or hydrostatic pressure caused by mineralizing hydrothermal fluids (Babae and Ganji, 2018).

Additionally, the hematite observed flow texture in hand specimen indicate most probably a hydrothermal origin. Colloform banding texture of goethite with hematite being surrounded by silicate matrix, usually arises from precipitates from hot colloidal aqueous solutions or gels coming from below (Salem et al., 2012).

The minor oxide mineral is magnetite that is characterized by very small aggregate in the samples. Disseminated subhedral to anhedral grains of magnetite in silicate minerals of the host rock indicate the primary texture of magnetite. Where the ore minerals occur as an intergranular anhedral phase compared to other gangue minerals. In such cases, this ore mineral crystallizes later in the magmatic sequence than other gangue minerals (Craig et al., 1981).

The most dominant sulfide mineralization in the studied samples is pyrite, in the form of idiomorphic, euhedral and subhedral of disseminated pyrite crystals distributed within the framework of the silicate minerals. This texture reveals that sulfide minerals were derived from immiscible sulfide liquids (Ramdohr, 1981). Pyrite is mainly isotropic, except in some cases that reveals weak anisotropy, attributed to tectonic stress (Craig et al., 1981; Awadh, 2006; Ramdohr, 2013). Disseminated texture and well-formed crystals indicate primary formation of the ore minerals, and this feature characterizes both the oxide and the sulfide minerals (Edwards, 1960; Ramdohr, 1981).

In several occasions the pyrite grains display rim-replacement texture by hematite and goethite that indicates that hematite and goethite formed as secondary minerals; this alteration results in island texture (Fig. 7h and Fig. 8d, and f). This texture has been created as a result of surface weathering conditions that caused oxidation of the iron in mineral phase (Buckingham and Sommer, 1983).

Chalcopyrite is a primary sulfide occurring as small anhedral grains in many types of the studied volcanic rocks. Chalcopyrite shows irregular form scattered in the rock fabric or as inclusions in hematite and silicate minerals. In some cases, chalcopyrite is replaced by hematite, whereas in some cases magnetite is corroded and replaced by chalcopyrite indicating also a replacement origin for chalcopyrite by hydrothermal solution (Fig. 8g) ( Ogola,1987; Almodóvar et al., 2019).

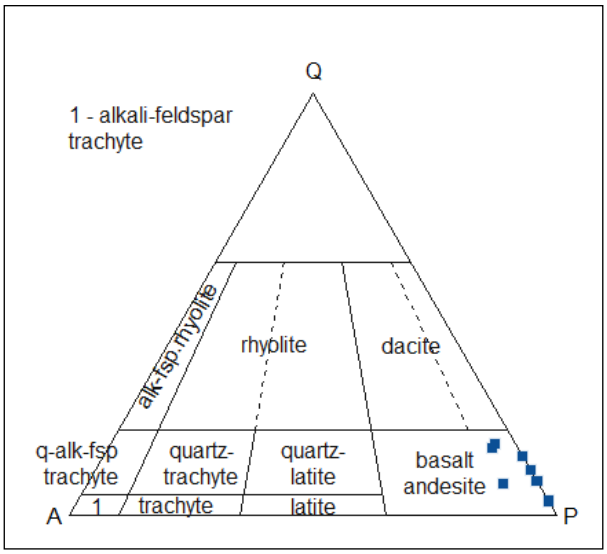


**Fig. 9.** Modal QAPF classification of volcanic rocks (Streckeisen, 1978). The corners of the double triangle are: Q = quartz; A = alkali feldspar; P = plagioclase; F=feldspathoid.

### 5.2. Geochemical Feature of the Host Rocks

The obtained results indicate that the Baska Piwaza volcanic rocks correspond basic to intermediate lithologies, and the correlation coefficients between major and trace elements provide information about their fractionation. The observed negative correlations between MgO and $Al_2O_3$, $Fe_2O_3$, CaO, $K_2O$, $P_2O_5$, $TiO_2$, Zr, and V, and positive correlations with $SiO_2$, MnO, $Na_2O$, Ni, and Cr; these correlations can be explained by the fractionation of plagioclase, clinopyroxene, amphibole, and Fe–Ti oxides (Fig. 10). Table (3) shows the correlation coefficients between different major elements and trace elements in a set of volcanic rock samples. The correlation coefficient between MgO and $Na_2O$ is 0.541, which is a positive correlation but not very strong. In contrast, the correlation coefficient between $Fe_2O_3$ and $TiO_2$ is 0.932, which is a very strong positive correlation. On the other hand, the correlation coefficient between $SiO_2$ and CaO is -0.877, which is a very strong negative correlation. Similarly, the correlation coefficient between MnO and $Al_2O_3$ is -0.666, which is a strong negative correlation (Table 3).

The ranges for Ni, Co and Cr in the Baska Piwaza samples are 36-243, 22-66, and 78-371 ppm, respectively (Table 2). Cr is highly compatible and is concentrated in clinopyroxene, and spinel (Wilson, 1989). Moreover, pyroxene, amphibole, and biotite are the three minerals that contain vanadium in their structures (Mason and Moore, 1985), and this explains the significant positive correlation with MgO (Figure 10 l). Ni shows positive correlation with MgO in all samples (Figure 10j). The studied samples contain vanadium in the range from 143-403 ppm. Vanadium exhibits a strong fractionation into the Fe–Ti oxides (Wilson, 1989). It shows a significant positive correlation with $Fe_2O_3$ (Figure 10m) which is related to the similarity in chemical behavior between V and Fe and the presence of relict magmatic Fe–Ti oxides in the rocks.

Some of volcanic samples are influenced by the hydrothermal alteration. The alteration effects on the volcanic rocks are consistent with the high value of loss on ignition (LOI) (3.7-11.1%) and high ratio of alkalis ($Na_2O+K_2O$) and petrography of the samples (Shanks III, 2010).

The tholeiitic nature is obvious from petrochemical discrimination diagrams of $SiO_2$ versus ($FeO_t$/MgO) after Miyashiro (1974) and AFM diagram after Irvine and Baragar (1971). The overall data indicate that the volcanic rocks have tholeiitic to calc-alkaline affinity (Fig. 11a and b).

The total alkali versus silica (TAS) diagram (Le Bas et al., 1986) was used, revealing that the studied samples fall in the basalt, basaltic andesite, basaltic trachyandesite fields (Fig. 11c). Furthermore, the $Na_2O+K_2O$ versus $SiO_2$ by Middlemost (1994) was applied, and it shows that all samples are plotted in basalt, basaltic andesite, and basalt –trachy andesite (Fig. 11d).

In general the studied samples are characterized by low K content (0.03 to 3.71%) and all samples are plotted within tholeiite-calc alkaline series except one sample that falls in shoshonite series according to Rickwood (1989) diagram (Fig. 11e). Additionally, similar results are obtained by using the $TiO_2$-MnO-$P_2O_5$ diagram by Mullen (1983), that indicates that all samples are plotted in the calc-alkaline and island arc tholeiitic (Fig. 11f).

The FeO*/MgO vs $TiO_2$ variation plot for the studied samples shows that all samples plot in the arc system (Fig. 11g). According to Rapela and Kay (1988); Aragón et al. (2013) the magmatic rocks in the fore- and back-arc have trace elements concentrations with small relative enrichment of some large-ion lithophile elements (Ba and Th) and the Ba/Nb ratio will be in the range of 50-100. Furthermore, the Ba vs. Nb diagram was utilized to confirm the depiction of arc signatures in these volcanic rocks, and their arc signatures were compared to those of the south Andes arc volcanic rocks (SAVZ) after Aragón *et al.* (2013) and shows that all samples have Ba/Nb ratio in the range of 50-100 with an average 85.41 and fall in the SAVZ field (Fig. 11h ).

The studied sample of radiolarian chert is characterized by low concentration of $SiO_2$ (45.8 wt.%) and high concentration of $Fe_2O_3$ (18.4 wt.%). High iron contents can indicate a strong hydrothermal influence during sedimentation. (Halamić et al. 2001).

Weil (1984, 1993) claims that only a small number of ions can substitute for $Si^{4+}$ and structural incorporation in a normal $Si^{4+}$ lattice position was proved for $Al^{3+}$, $Ga^{3+}$,$Fe^{3+}$, $Ge^{4+}$, $Ti^{4+}$, and $P^{5+}$. According to earlier research, the considerable inclusion of Ti in the crystal lattice of quartz occurs at high temperatures (Wark and Watson 2006). $TiO_2$ in the quartz vein samples is 0.01 wt.% and, the concentration of $Fe_2O_3$ is 0.04 wt.%. The microscope studies of the quartz veins did not show rutile, illminite and iron oxide mineralizations as inclusions in quartz crystal. Therefore, the $TiO_2$ concentration in this quartz samples is probably incorporated in the structure of the quartz veins at low temperature condition (Mirza et al., 2022). In addition the titanium concentration in studied quartz is similar to that of hydrothermal quartz described by Manalo et al. (2020).

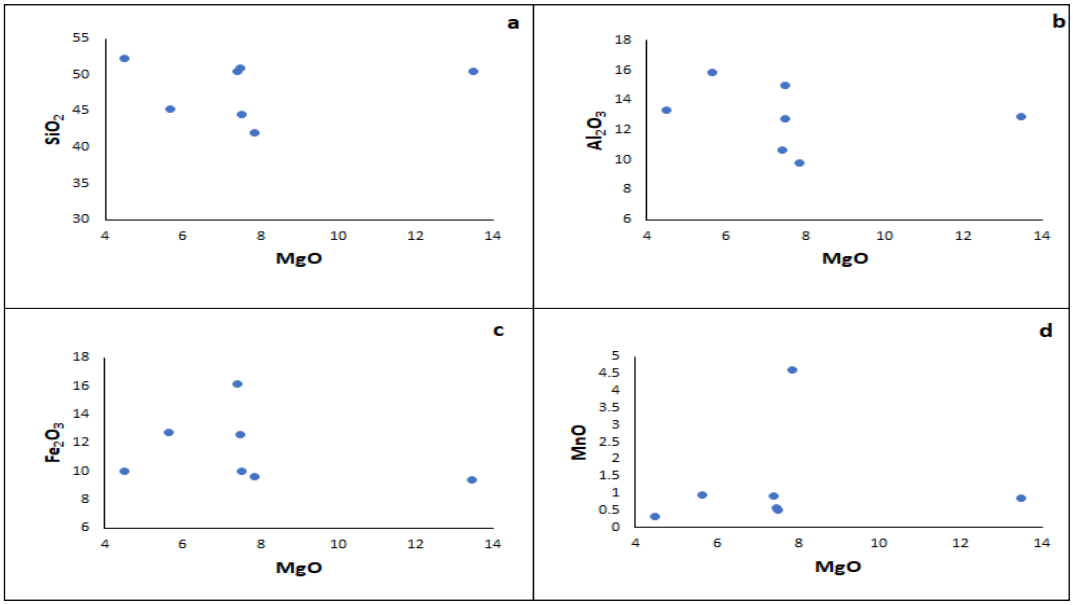

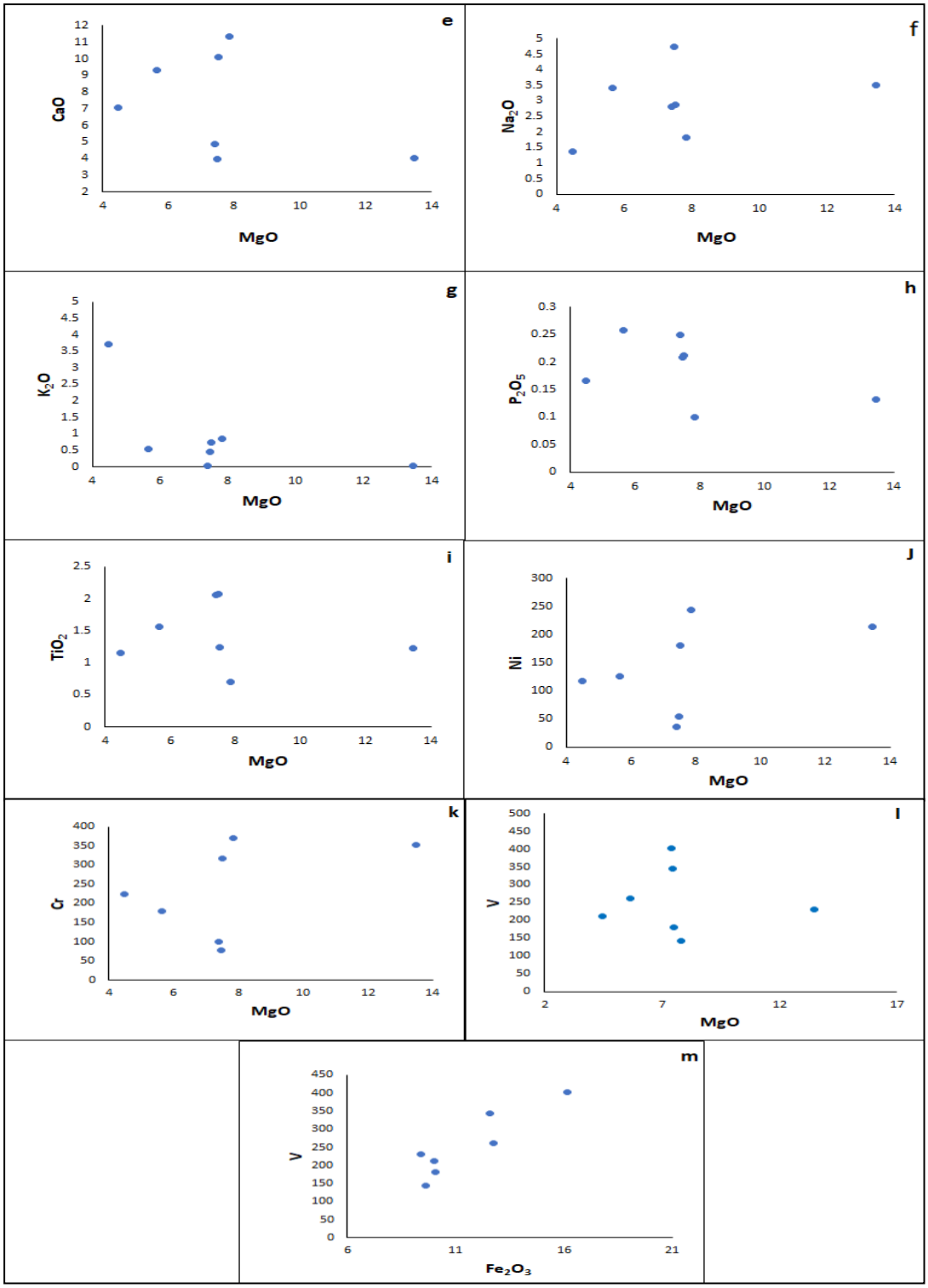


**Fig. 10.** Selected binary diagrams showing major and trace elements variation of Baska Piwaza volcanic rocks.

**Table 3.** Correlation coefficient for the studied volcanic samples.

| | $SiO_2$ | $TiO_2$ | $Al_2O_3$ | $Fe_2O_3$ | MnO | MgO | CaO | $Na_2O$ | $K_2O$ | $P_2O_5$ | V | Cr | Ni |
|---|---|---|---|---|---|---|---|---|---|---|---|---|---|
| $SiO_2$ | 1 | | | | | | | | | | | | |
| $TiO_2$ | 0.410 | 1 | | | | | | | | | | | |
| $Al_2O_3$ | -0.005 | 0.118 | 1 | | | | | | | | | | |
| $Fe_2O_3$ | 0.222 | 0.932 | -0.143 | 1 | | | | | | | | | |
| MnO | -0.666 | -0.555 | -0.666 | -0.232 | 1 | | | | | | | | |
| MgO | 0.072 | -0.178 | -0.205 | -0.264 | 0.102 | 1 | | | | | | | |
| CaO | -0.877 | -0.488 | 0.126 | -0.318 | 0.537 | -0.467 | 1 | | | | | | |
| $Na_2O$ | -0.045 | 0.433 | 0.450 | 0.268 | -0.358 | 0.541 | -0.313 | 1 | | | | | |
| $K_2O$ | 0.357 | -0.317 | 0.127 | -0.354 | -0.193 | -0.614 | 0.115 | -0.773 | 1 | | | | |
| $P_2O_5$ | 0.183 | 0.861 | 0.362 | 0.827 | -0.514 | -0.598 | -0.086 | 0.235 | -0.034 | 1 | | | |
| V | 0.533 | 0.951 | -0.124 | 0.926 | -0.434 | -0.043 | -0.649 | 0.350 | -0.316 | 0.718 | 1 | | |
| Cr | -0.441 | -0.898 | -0.1001 | -0.893 | 0.483 | 0.5268 | 0.338 | -0.092 | -0.049 | -0.928 | -0.861 | 1 | |
| Ni | -0.560 | -0.899 | -0.066 | -0.856 | 0.569 | 0.486 | 0.434 | -0.037 | -0.109 | -0.877 | -0.871 | 0.977 | 1 |

Strong Correlation  No correlation  Weak correlation

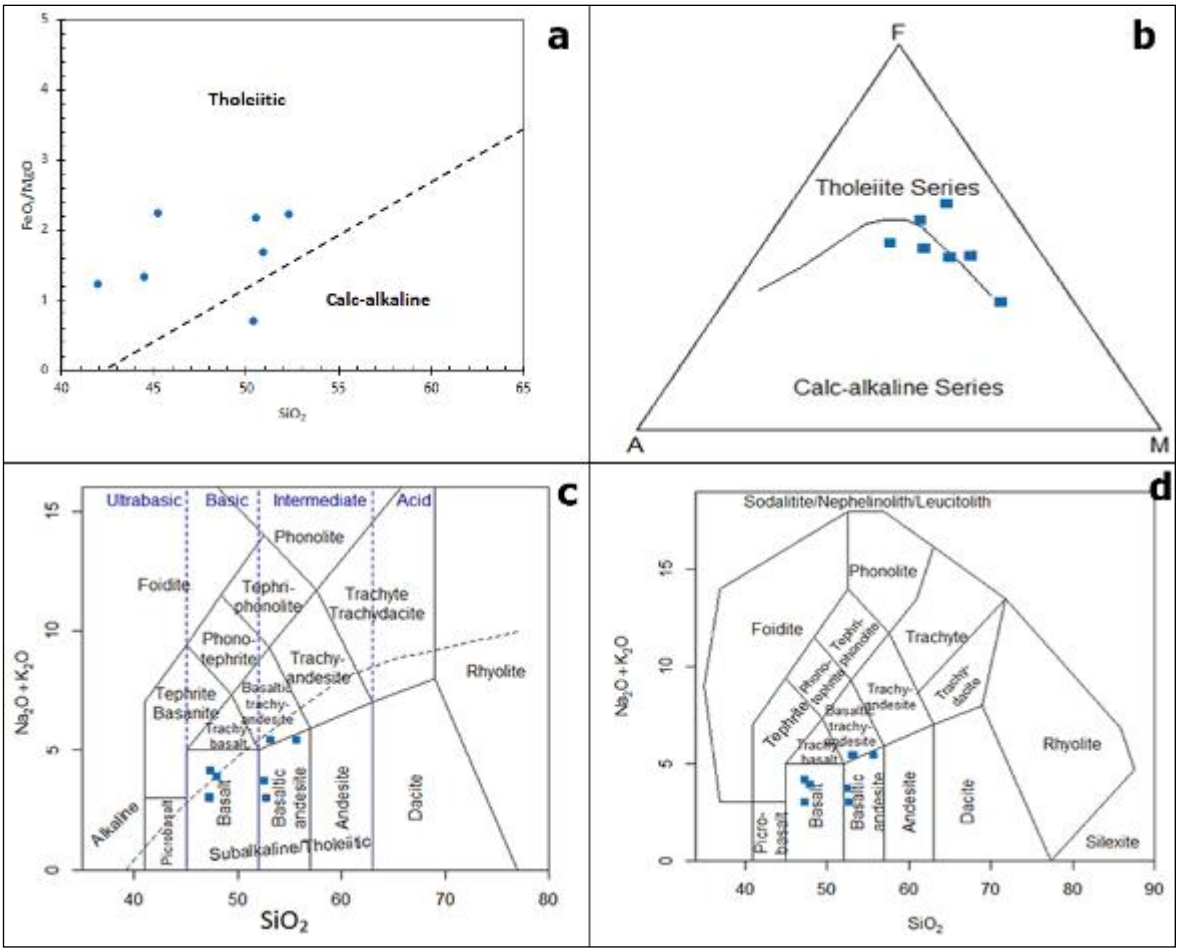

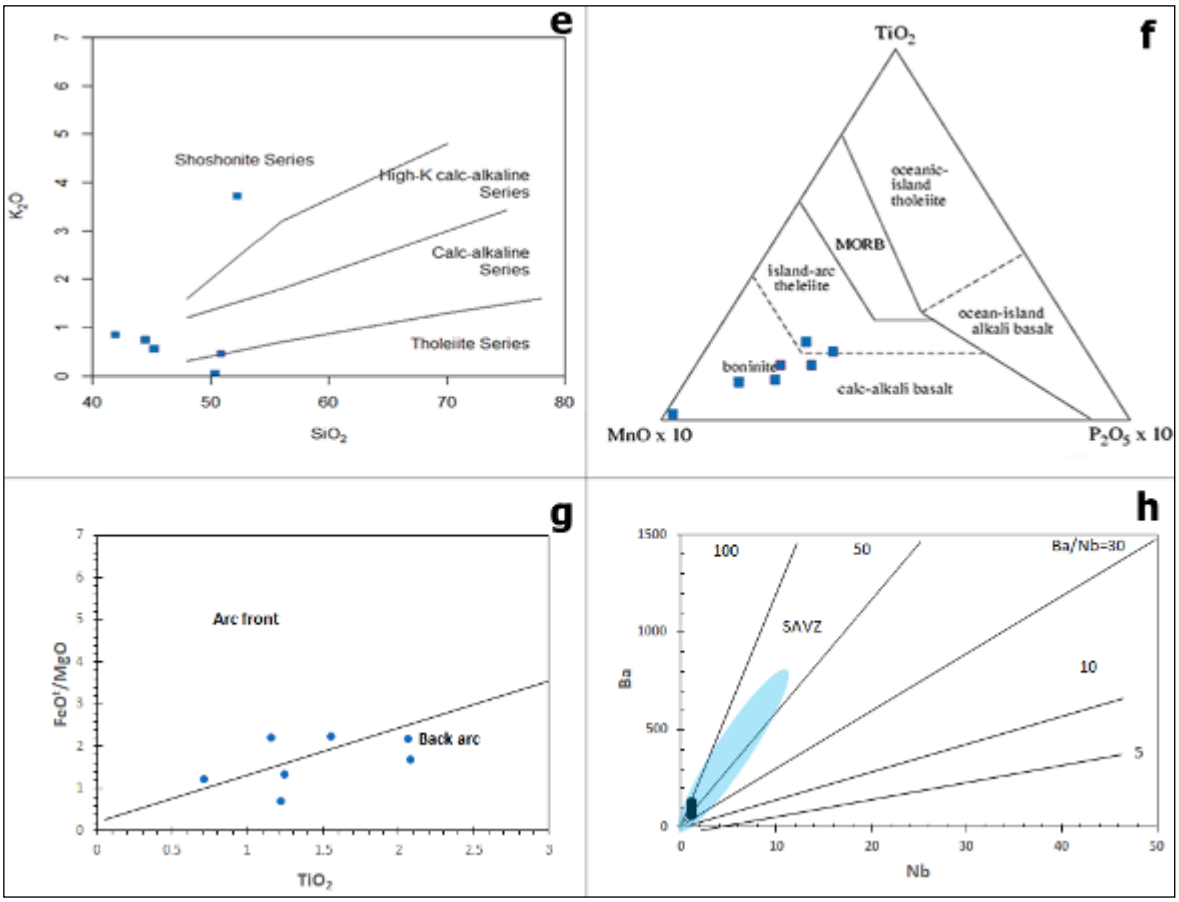


**Fig. 11.** (**a)** $SiO_2$ versus ($FeO_t$/MgO) diagram of (Miyashiro, 1974). (**b)** AFM diagram (Irvin and Baragar, 1971). (**c)** $Na_2O + K_2O$ vs. $SiO_2$ (Le Bas et al. 1986). (**d)** $Na_2O + K_2O$ vs. $SiO_2$ (Middlemost.1994). (**e):** $K_2O$ vs. $SiO_2$ (Rickwood. 1989). (**f)** MnO–$TiO_2$ –$P_2O_5$ discrimination diagram, after Mullen (1983). (**g)** FeO*/MgO vs $TiO_2$ variation diagram. (**h)** Ba vs. Nb diagram for arc front volcanic rocks, (SAVZ) field represent south Andes volcanic rocks after (Aragon et al., 2013).

### 5.3. Mineral Paragenesis Revise

In general, there are two main stages of ore mineralization that can be recognized under three-time epochs (Fig. 12). The paragenetic minerals originated from the hydrothermal signals that produce the epigenetic ore minerals-filled veins and fissures to the alteration and replacement processes that occurred under the hydrothermal and surface weathering conditions. These conditions resulted in high alterations of the primary sulfide minerals that formed the recent secondary ores.

The silicate minerals such as (plagioclase, augite, amphibole, K-feldspar, muscovite, and quartz) are essential minerals in volcanic rocks, being early forming minerals. The chloritization and sericitization, are the dominant secondary minerals that occur by the alteration of the host rocks. From the petrographically study it is revealed that the sericitization occurred from the alteration of plagioclase, whereas chloritization happened by the alteration of mafic minerals. In addition, pyroxene in several cases is altered and replaced by chlorite. The presences of prehnite and pumpellyite indicate low-grade metamorphism affected some of the studied samples. The primary oxide minerals are hematite and magnetite present as prismatic and lath shape being replaced by goethite. The primary sulfide minerals are pyrite and chalcopyrite being present as well-formed crystals and being characterized by disseminated textures that indicate early mineralization. Additionally, pyrite also replaced by goethite. Irregular pyrite indicates later mineralization stage. Moreover, chalcopyrite replaced hematite and magnetite, defining also a later stage mineralization of chalcopyrite.

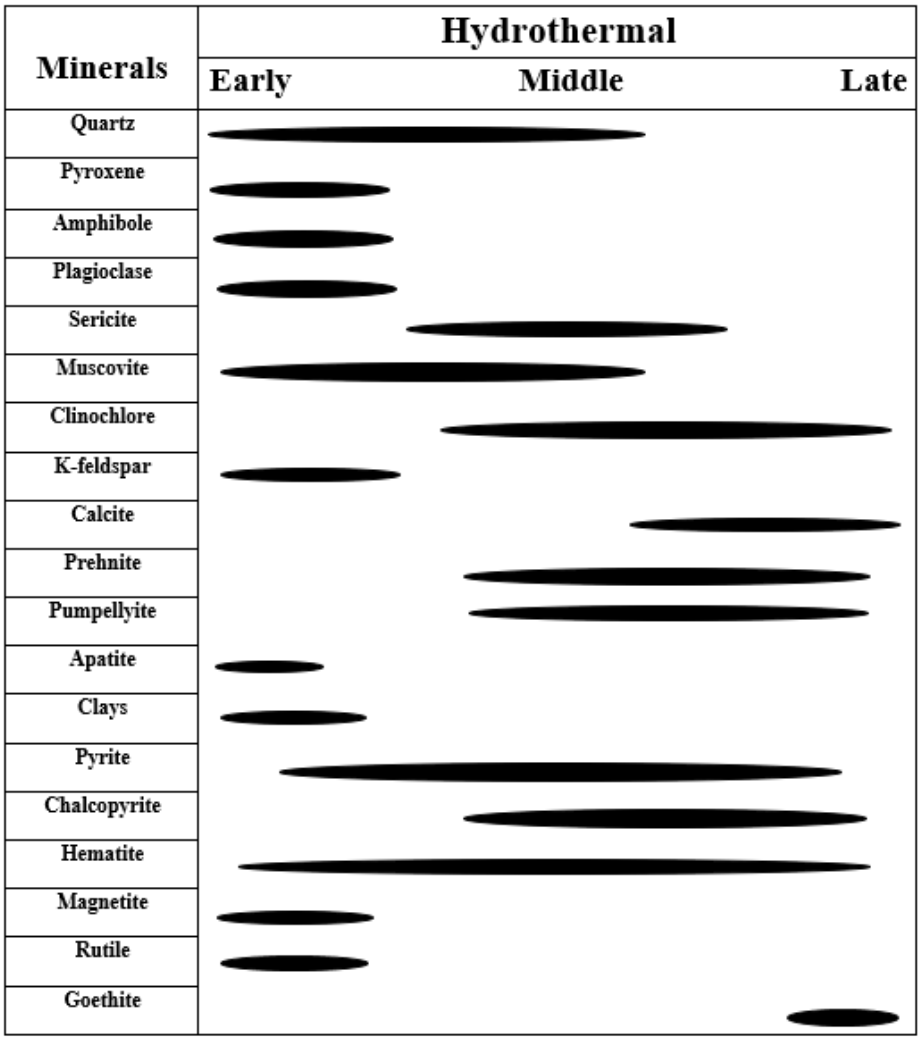


**Fig 12**. Paragenesis of silicate and ore minerals of studied samples.

## 6. Conclusions

Volcanic igneous and sedimentary rocks were studied in Baska Piwaza section of Halgurd mountain. According to the field observation, petrographical and geochemical data, the volcanic rocks are basalt to andesite, being characterized by aphanitic, porphyritic, glomeroporphyritic, vesicular, and amygdaloidal textures. Based on the geochemical data the volcanic rocks have tholeiitic to calc-alkaline affinity. Radiolarian chert is the only sedimentary rock in the area, being characterized by high percentage of iron oxide (18.4%) and hematite (23%). Ore microscopy shows that the samples contain sulfide and oxide ore minerals, with the iron-oxides being the most abundant ore minerals in the Baska Piwaza section. The dominant oxide ore mineral is hematite, with minor participation of magnetite goethite and rutile. Additionally, the dominant sulfide ore mineral is pyrite, with secondary participation of chalcopyrite. Chalcopyrite is the only copper bearing mineral in the studied samples.

High value of loss on ignition (LOI) and high ratio of alkalis ($Na_2O+K_2O$) indicate that the studied section is influenced by hydrothermal alteration. Chloritization and sericitization are the dominant alteration of the host rocks. The petrographical study revealed that the sericitization affected mostly the plagioclases, whereas chloritization the mafic minerals. These observations lead to the conclusion that the volcanic rocks in the Baska Piwaza section were affected by hydrothermal metamorphism that resulted in alteration and resorption.

Low concentration of $SiO_2$ (45.8 wt.%) and high concentration of $Fe_2O_3$ (18.4 wt.%) in the radiolarian chert sample indicate the effect of hydrothermal fluid during sedimentation of radiolarian chert. Besides, low concentration of $TiO_2$, and $Fe_2O_3$ indicate the quartz vein was formed due to low hydrothermal solution.

Two main stages of ore mineralization can be identified under three – time epochs which are early, middle, and late stage caused the formation of oxide and sulfides ore minerals. This paragenetic minerals originated from the hydrothermal signals that produce the epigenetic ore minerals-filled veins and fissures to the supergene enrichment processes that occurred under the surface weathering conditions.

## References

Ahmed, I.N., Kettanah, Y.A. and Ismail, S.A., 2020. Genesis and tectonic setting of high-Cr podiform chromitites of the Rayat ophiolite in the Zagros Suture Zone, northeastern Iraq. Ore Geology Reviews, 123.

Al-Banna, N.Y. and Al-Mutwali, M.M., 2008. Microfacies and age determination of the sedimentary sequences within Walash volcano-sedimentary Group, Mawat Complex, northeast Iraq. Tikrit Journal of Pure Science, 13(3), 46-52.

Al-Bassam, K.S., 2013. Mineral resources of Kurdistan region, Iraq. Iraqi Bulletin of Geology and Mining, 9(3), 103-127.

Ali, S. A. and Aswad, K., 2013. SHRIMP U-Pb dating of zircon inheritance in Walash arc volcanic rocks (Paleogene age), Zagros Suture Zone, NE Iraq: new insights into crustal contributions to trachytic andesite generation. Iraqi National Journal of Earth Science, 13(1), 45-58.

Ali, S.A., Buckman, S., Aswad, K.J., Jones, B.G., Ismail, S.A. and Nutman, A.P., 2013. The tectonic evolution of a N eo-T ethyan (E ocene–O ligocene) island-arc (W alash and N aopurdan groups) in the K urdistan region of the N ortheast I raqi Z agros S uture Z one. Island Arc, 22(1), 104-125.

Al-Mehiadi, H., 1974. Geological investigation of Mawat – Chowarta area, northeastern Iraq.

Almodóvar, G.R., Yesares, L., Sáez, R., Toscano, M., González, F. and Pons, J.M., 2019. Massive sulfide ores in the Iberian Pyrite Belt: Mineralogical and textural evolution. Minerals, 9(11), 653.

Alt, J.C., Laverne, C., Vanko, D.A., Tartarotti, P., Teagle, D.A., Bach, W., Zuleger, E., Erzinger, J., Honnorez, J., Pezard, P.A. and Becker, K.H.S.M., 1996. Hydrothermal alteration of a section of upper oceanic crust in the Eastern Equatorial Pacific: A synthesis of results from Site 504 (DSDP Legs 69, 70, and 83, and ODP Legs 111, 140, and 148). In Proceedings of the ocean drilling program: scientific results, 148, 417-434.

Aragón, E., Pinotti, L., Fernando, D., Castro, A., Rabbia, O., Coniglio, J., Demartis, M., Hernando, I., Cavarozzi, C.E. and Aguilera, Y.E., 2013. The Farallon-Aluk ridge collision with South America: Implications for the geochemical changes of slab window magmas from fore-to back-arc. Geoscience Frontiers, 4(4), 77-388.

Aswad, K.J. and Elias, E.M., 1988. Petrogenesis, geochemistry and metamorphism of spilitized subvolcanic rocks of the Mawat Ophiolite Complex, NE Iraq. Ofioliti, 13(2/3), 95-109.

Aswad, K.J., 1999. Arc-continent collision in Northeastern Iraq as evidenced by Mawat and Penjwin Ophiolite Complexes. Raffidain Journal of Science, 10, 51-61.

Awadh, S.M., 2006. Mineralogy, geochemistry and origin of the zinc–lead–barite deposits from selected areas from north of Zakho, Northern Iraq. Unpublished Ph. D. Thesis (in Arabic), University of Baghdad, College of Science, Department of Geology, 191.

Aziz, N.R., Elias, E.M. and Aswad, K.J., 2011. Rb–Sr and Sm–Nd isotope study of serpentinites and their impact on the tectonic setting of Zagros Suture Zone, NE-Iraq. Iraqi Bulletin of Geology and Mining, 7(1), 67-75.

Babaei, A.H. and Ganji, A., 2018. Characteristics of the Ahmadabad hematite/barite deposit, Iran–studies of mineralogy, geochemistry and fluid inclusions. Geologos, 24(1), 55-68.

Bolton, C.M.G., 1958. The Geology of Ranyia area. Unpublished, Site Inves. Company report, SOM Library, Baghdad.

Buckingham, W.F. and Sommer, S.E., 1983. Mineralogical characterization of rock surfaces formed by hydrothermal alteration and weathering; application to remote sensing. Economic Geology, 78(4), 664-674.

Craig, J.R., Vaughan, D.J. and Hagni, R.D., 1981. Ore Microscopy and Ore Petrography (Vol. 406). New York: Wiley.

Edwards, A.B., 1960. Textures of the Ore Minerals. The Australian Institute of Mining and Metallurgy. Victoria.

Fouad, S.F., 2015. Tectonic map of Iraq, scale 1: 1000 000, 2012. Iraqi Bulletin of Geology and Mining, 11(1), 1-7.

Halamić, J.O.S.I.P., Marchig, V.E.S.N.A. and Goričan, Š., 2001. Geochemistry of Triassic radiolarian cherts in north-western Croatia. Geologica Carpathica, 52(6), 327-342

Heiri, O., Lotter, A.F. and Lemcke, G., 2001. Loss on ignition as a method for estimating organic and carbonate content in sediments: reproducibility and comparability of results. Journal of paleolimnology, 25, 101-110.

Irvine, T.N. and Baragar, W.R.A., 1971. A guide to the chemical classification of the common volcanic rocks. Canadian journal of earth sciences, 8(5), 523-548.

Ismail, S.A., Arai, S., Ahmed, A.H. and Shimizu, Y., 2009. Chromitite and peridotite from Rayat, northeastern Iraq, as fragments of a Tethyan ophiolite. Island Arc, 18(1), 175-183.

Ismail, S.A., Kettanah, Y.A., Chalabi, S.N., Ahmed, A.H. and Arai, S., 2014. Petrogenesis and PGE distribution in the Al-and Cr-rich chromitites of the Qalander ophiolite, northeastern Iraq: Implications for the tectonic environment of the Iraqi Zagros Suture Zone. Lithos, 202, 21-36.

Jassim, S.Z. and Goff, J.C. eds., 2006. Geology of Iraq. DOLIN, sro, distributed by Geological Society of London.

Koyi, A.M., 2006. Petrochemistry, petrogenesis and Isotope dating of Walash volcanic rocks at Mawat-Chowarta area, NE Iraq. Unpublished MSc. Thesis, Universty of Mosul.

Le Bas, M.L., Maitre, R.L., Streckeisen, A., Zanettin, B. and IUGS Subcommission on the Systematics of Igneous Rocks, 1986. A chemical classification of volcanic rocks based on the total alkali-silica diagram. Journal of petrology, 27(3), 745-750.

Manalo, P.C., Subang, L.L., Imai, A., de los Santos, M.C., Takahashi, R. and Blamey, N.J., 2020. Geochemistry and fluid inclusions analysis of vein quartz in the multiple hydrothermal systems of Mankayan mineral district, Philippines. Resource Geology, 70(1), 1-27

Mason, B. and Moore, C.B., 1985. Principles of geochemistry.

Middlemost, E.A., 1994. Naming materials in the magma/igneous rock system. Earth-science reviews, 37(3-4), 215-224.

Minerstry of natural resources. 2016. Occurrences of metallic deposits in the Kurdistan Region - Iraq Kurdistan Regional Government.

Mirza, T.A., Salih, N.M., Delpomdor, F.R., Kalaitzidis, S.P. and Rashid, S.G., 2022. Formation of quartz veins within Serginil Phyllite Group-Penjween area, Iraqi Kurdistan Region: insights from geochemical and fluid inclusion data. Arabian Journal of Geosciences, 15(9), 887.

Miyashiro, A., 1974. Volcanic rock series in island arcs and active continental margins. American journal of science, 274(4), 321-355

Mohammed, F. A., 2006. Petrography, heavy mineral study and tectonic setting of Walash Naopurdan Series Sandstones, Qalander area, Northeastern Iraq. College of Science Salahaddin University.

Montgomery, H. and Kerr, A.C., 2009. Rethinking the origins of the red chert at La Désirade, French West Indies. Geological Society, London, Special Publications, 328(1), 457-467.

Moores, E.M., Kellogg, L.H. and Dilek, Y., 2000. Tethyan ophiolites, mantle convection, and tectonic" historical contingency": A resolution of the" ophiolite conundrum". Special Papers-Geological Society of America, 3-12.

Mullen, E.D., 1983. MnO/TiO2/P2O5: a minor element discriminant for basaltic rocks of oceanic environments and its implications for petrogenesis. Earth and planetary science letters, 62(1), 3-62.

Numan, N.M., 1997. A plate tectonic scenario for the Phanerozoic succession in Iraq. Iraqi Geological Journal, 30(2), 85-110.

Ogola, J.S., 1987. Mineralization in the migori greenstone belt, macalder, Western Kenya. Geological Journal, 22(S2), 25-44.

Pirouei, M., Kolo, K. and Kalaitzidis, S.P., 2020a. Chromium-rich muscovite mineralization in Zagros ophiolites in Iraqi Kurdistan: a study on fuchsite paragenetic association with listvenite types. Arabian Journal of Geosciences, 13, 1-13.

Pirouei, M., Kolo, K. and Kalaitzidis, S.P., 2020b. Hydrothermal listvenitization and associated mineralizations in Zagros Ophiolites: Implications for mineral exploration in Iraqi Kurdistan. Journal of Geochemical Exploration, 208, 106404.

Pirouei, M., Kolo, K., Kalaitzidis, S.P. and Abdullah, S.M., 2021. Newly discovered gossanite-like and sulfide ore bodies associated with microbial activity in the Zagros ophiolites from the Rayat area of NE Iraq. Ore Geology Reviews, 135, 104191.

Ramdohr, P., 1981. The Ore Minerals And Their Intergrowth. Pergamon Press., New York, 1202.

Ramdohr, P., 2013. The Ore Minerals and their Intergrowths. Elsevier.

Rapela, C.W. and Kay, S.M., 1988. Late Paleozoic to Recent magmatic evolution of northern Patagonia. Episodes Journal of International Geoscience, 11(3), 175-182.

Richards, H.G. and Boyle, J.F., 1986. Origin, alteration and mineralization of inter-lava metalliferous sediments of the Troodos Ophiolite, Cyprus. In Conference metallogeny of basic and ultrabasic rocks, 21-31.

Rickwood, P.C., 1989. Boundary lines within petrologic diagrams which use oxides of major and minor elements. lithos, 22(4), 247-263.

Salem, I.A., Ibrahim, M.E. and Abd El Monsef, M., 2012. Mineralogy, geochemistry, and origin of hydrothermal manganese veins at Wadi Maliek, Southern Eastern Desert, Egypt. Arabian Journal of Geosciences, 5(3), 385.

Shanks III, W.C., 2010. Hydrothermal alteration in volcanogenic massive sulfide occurrence model. US Geological Survey Scientific Investigations Report, 5070, 12.

Sissakian, V.K., 2000. Geological Map of Iraq, 3rd edit., scale 1: 1000 000, Baghdad, Iraq.

Streckeisen, A., 1978. IUGS Subcommission on the Systematics of Igneous Rocks. Classification and Nomenclature of Volcanic Rocks, Lamprophyres, Carbonatites and Melilite Rocks. Recommendations and Suggestions. Neues Jahrbuch fur Mineralogie. Stuttgart. Abhandlungen, 143, 1-14.

Wark, D.A. and Watson, E.B., 2006. TitaniQ: a titanium-in-quartz geothermometer. Contributions to Mineralogy and Petrology, 152(6), 743-754.

Weil, J.A., 1984. A review of electron spin spectroscopy and its application to the study of paramagnetic defects in crystalline quartz. Physics and Chemistry of Minerals, 10(4), 149-165.

Weil, J.A., 1993. A review of the EPR spectroscopy of the point defects in α-quartz: The decade 1982–1992. The Physics and Chemistry of SiO 2 and the Si-SiO 2 Interface 2, 131-144.

Whitney, D.L. and Evans, B.W., 2010. Abbreviations for names of rock-forming minerals. American mineralogist, 95(1), 185-187.

Wilson, M. ed., 1989. Igneous petrogenesis. Dordrecht: Springer Netherlands.